BEST AVAILABLE IMAGES

Defective images within this document are accurate representations of the original documents submitted by the applicant.

Defects in the images may include (but are not limited to):

- BLACK BORDERS
- TEXT CUT OFF AT TOP, BOTTOM OR SIDES
- FADED TEXT
- ILLEGIBLE TEXT
- SKEWED/SLANTED IMAGES
- COLORED PHOTOS
- BLACK OR VERY BLACK AND WHITE DARK PHOTOS
- GRAY SCALE DOCUMENTS

IMAGES ARE BEST AVAILABLE COPY.

As rescanning documents *will not* correct images, please do not report the images to the Image Problem Mailbox.

Crystallization behavior of Ge-doped eutectic $Sb_{70}Te_{30}$ films in optical disks

Pramod K. Khulbe, Terril Hurst, Michikazu Horie, and Masud Mansuripur

We report laser-induced crystallization behavior of binary Sb–Te and ternary Ge-doped eutectic $Sb_{70}Te_{30}$ thin film samples in a typical quadrilayer stack as used in phase-change optical disk data storage. Several experiments have been conducted on a two-laser static tester in which one laser operating in pulse mode writes crystalline marks on amorphous film or amorphous marks on crystalline film, while the second laser operating at low-power cw mode simultaneously monitors the progress of the crystalline or amorphous mark formation in real time in terms of the reflectivity variation. The results of this study show that the crystallization kinetics of this class of film is strongly growth dominant, which is significantly different from the crystallization kinetics of stochiometric Ge–Sb–Te compositions. In Sb–Te and Ge-doped eutectic $Sb_{70}Te_{30}$ thin-film samples, the crystallization behavior of the two forms of amorphous states, namely, as-deposited amorphous state and melt-quenched amorphous state, remains approximately same. We have also presented experiments showing the effect of the variation of the Sb/Te ratio and Ge doping on the crystallization behavior of these films.

OCIS codes: 210.0210, 210.4810.

1. Introduction

In the phase diagram of the ternary alloy system of Ge–Te–Sb are stoichiometric $Ge_2Sb_2Te_5$, $GeSb_2Te_4$, and $GeSb_4Te_7$ materials, which fall along the GeTe–Sb_2Te_3 line in the phase diagram of the ternary alloys system. These compositions form the basis of phase-change (PC) recording method in optical data storage, which have rapid crystallization properties (crystallization time is ~ 20 ns) and user data rates ~ 35 megabits per second.[1] The crystallization kinetics of these materials is predominantly nucleation driven, which is defined by the formation of a large number of crystallization centers, or nuclei, and their subsequent growth into a large number of small crystalline clusters. This happens above a certain temperature called the crystallization temperature. Ag–In–Sb–Te-based materials that have a composition close to the eutectic $Sb_{70}Te_{30}$ are also being used in PC optical recording in which some of the Te is replaced by Ag and In. The chemical structure of Ag–In–Sb–Te-based materials in an ordered state was found to be $(Ag–Sb–Te)_x$ $(In_{1-y}Sb_y)_{1-x}$.[2] These materials show growth-dominated crystallization kinetics, which means that above the crystallization temperature there is relatively a small probability of nuclei formation, however, once nuclei are formed they grow very rapidly. In the third category of materials, instead of replacing Te by Ag and In, one could replace Te by Ge and (or) Sb to obtain another set of materials with higher growth probabilities in their crystallization kinetics.[3] A recent report shows that the addition of approximately 10% Ge to the eutectic $Sb_{70}Te_{30}$+Sb (SGT) composition results in a nucleation-free and pure growth-dominated crystallization process.[4] The advantage of nucleation-free characteristics of SGT compositions is low jitter and very high amorphous phase stability. The low jitter in this type of media is due to the fact that the written amorphous marks are sharply defined along the crystal boundary, which in the case of stoichiometric materials are defined by a gradual change in the density and size of the many small crystallites. As mentioned earlier, crystallization is a two-step process that involves formation of several small nuclei followed by their growth into large crystalline clusters. In absence of the nuclei, growth cannot occur. Because these materials have extremely low nucleation probability, this leads to a very important property for data storage application, which is a high

Authors P. K. Khulbe (pkkhulbe@u.arizona.edu), T. Hurst, and M. Mansuripur are with the Optical Science Center, University of Arizona, Tucson, Arizona 85721. M. Horie is with Mitsubishi Chemical Corporation, Yokohama Information and Electronics Research Center, Storage Media Laboratory 1000, Kamoshida-cho Aoba-ku Yokohama 227-8502, Japan.

Received 24 January 2002; revised manuscript received 29 May 2002.

0003-6935/02/296220-10$15.00/0

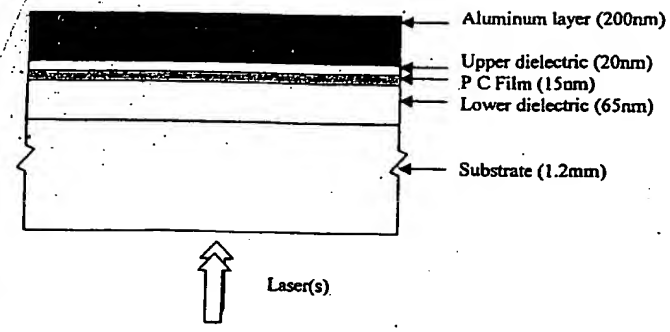

Fig. 1. Typical quadrilayer PC optical disk used in the present study. Two laser beams are focused on the PC layer at the same spot from the substrate side. One laser is pulsed, while the other, operating in cw mode, monitors in real time the reflectivity variation caused by pulse laser heating.

amorphous phase (or data bit) stability. This property also seems to be useful for a long data-retention time and would enable us to write smaller marks for achieving higher storage density. A control over the mark size also makes these materials attractive for multilevel and analog recording. In our previous articles we presented a detailed experimental study of the crystallization behavior of a stoichiometric $Ge_2Sb_{2.3}Te_5$ material, which showed nucleation-dominated crystallization kinetics.[5,6] In this paper, we present another set of experiments conducted to understand the crystallization kinetics of several binary (Sb–Te) and ternary (Ge doped Sb–Te) materials having compositions close to the eutectic point ($Sb_{70}Te_{30}$) in the phase diagram of a ternary Ge–Sb–Te alloy system.

2. Experiments

All samples used in various experiments presented in this paper have a typical quadrilayer disk structure as shown in Fig. 1. Crystallization and amorphization experiments were conducted on a two-laser static tester, which is equipped with two semiconductor lasers operating at $\lambda_1 = 680$ nm (laser 1) and $\lambda_2 = 643$ nm (laser 2).[7] Both lasers are focused simultaneously and coincidently on the PC layer of the sample through a microscope objective of 0.6 NA from the substrate side. The microscope objective has a correction for substrate thickness and gives a focus spot of ~ 0.82 μm diameter at FWHM ($\lambda = 680$ nm). The light reflected from the sample is collected by the same microscope objective and then passed through a glass prism, which separates two wavelengths. Both wavelengths are detected and fed to a digital oscilloscope and a computer for further processing. Both lasers can be operated independently in pulse and cw mode. However, in most experiments presented here we used laser 1 in variable pulse-power and pulse-duration mode to create crystalline marks on amorphous films and melt-quenched amorphous marks on crystalline films. The mark formation process is monitored by measuring real-time reflectivity variation using laser 2, which operates in low-power cw mode at ~ 0.2 mW. Reflectivity variation during mark formation occurs because of the difference in the optical constants (n and k) of amorphous and crystalline states of the PC material. Various layer thicknesses in a quadrilayer structure (Fig. 1) are optimized to give a required reflectivity difference for amorphous and crystalline states of the PC film, while maintaining a requisite thermal property of the stack.[8] A detailed description of the two-laser static tester system is reported in one of our previous publications.[7]

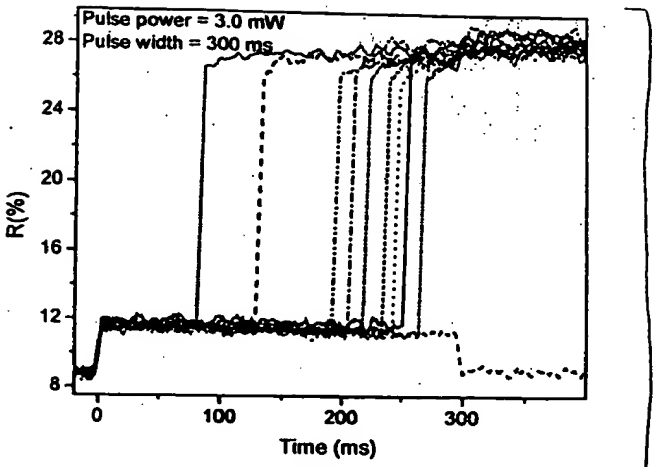

Fig. 2. Ten reflectivity traces obtained during crystalline mark formation on as-deposited $Ge_5Sb_{68}Te_{27}$ film in a quadrilayer structure. All crystalline marks were written by 3.0-mW laser pulses. The pulse duration was 300 ms (0–300 ms along the x axis). Reflectivity variation is monitored by 0.2-mW cw laser beam from the second laser.

3. Results

A. Crystalline-Mark Formation on As-Deposited Amorphous Film

Figure 2 shows ten reflectivity traces obtained during crystalline-mark formation on as-deposited amorphous film of $Ge_5Sb_{68}Te_{27}$ PC material incorporated in a typical quadrilayer structure shown in Fig. 1. These reflectivity traces were obtained by applying ten identical laser pulses from laser 1 at ten different spots on the film. All laser pulses had 3.0 mW power and 300 ms width (0–300 ms on the x axis). In Fig. 2, we see a rise in reflectivity at the beginning of the laser pulse ($t = 0$) in all reflectivity traces and another jump in reflectivity, which occurs randomly during the pulse. Crystallization occurs during the second jump. In one of the situations where there is no second jump in the reflectivity trace and the reflectivity returns to its pre-pulse value is associated with no crystalline mark formation. Such random jumps in reflectivity traces and an existence of a large nucleation time before the onset of crystallization are unique to phase change materials, which show growth-dominated crystallization kinetics. In contrast to this behavior, in a typical nucleation-dominated $Ge_2Sb_{2.3}Te_5$ material the crystalline mark

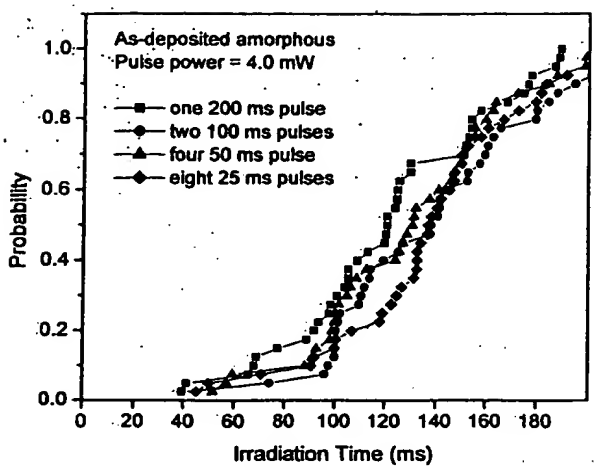

Fig. 3. Probability of crystallization versus irradiation time for various 4.0-mW laser-pulse schemes. In the case of irradiation from multiple pulses, the time interval in between pulses is a few seconds and is not counted in the total irradiation time.

formation process is indicated by a nonrandom and a gradual increase in the reflectivity within a few tens of ns after the onset of the laser pulse, and the crystallization gets completed before ~ 1.0 μs.[5] The reflectivity traces shown in Fig. 2 indicate that there is a very small probability of nucleation, however, once a nucleation center is formed it grows very rapidly in crystalline clusters raising the reflectivity abruptly. In the event of no crystallization, the reflectivity drops to its amorphous-state value indicating that no nucleation center could be formed during the pulse. The rise in reflected signal (~ 3%) in the beginning of the pulse is not due to the crystalline mark formation but it is associated with the temperature dependence of optical constants of the PC film. This behavior is very frequently observed in quadrilayer stacks in which optical constants of one or more layers may vary by laser heating and thereby modifying the reflectivity of the stack.[9]

To further understand the crystallization behavior indicated by random jumps in reflectivity traces in Fig. 2, we conducted the following experiment. For a fixed-pulse power (4.0 mW) and fixed-pulse length (200 ms) we wrote 40 crystalline marks on as-deposited amorphous film, which produced 40 reflectivity traces, such as is shown in Fig. 2. On the basis of the position of jumps in these reflectivity traces, we evaluated the probability of crystalline mark formation for various values of pulse-irradiation time. A plot of total irradiation time versus the probability of crystalline mark formation is shown on Fig. 3 by filled-square data points. Now this 4.0 mW, 200 ms pulse was split into two 100-ms-long pulses separated by a time interval of a few seconds, and this two-pulse sequence is used to write another set of 40 crystalline marks. Few crystalline marks could be written during the first pulse, and most of the crystalline marks were written during the second pulse. A plot of accumulated irradiation time versus the probability of crystalline mark formation is also plotted in Fig. 3 by data points represented by filled circles. Here accumulated irradiation time is the time in which a focused laser pulse remains applied on a spot before crystallization occurs. For example, if a crystalline mark forms at 20 ms from the beginning of the second pulse, the accumulated irradiation time is 120 ms (100 ms during the first pulse plus 20 ms during the second pulse). Similar experiments were conducted for a pulse sequence of four 50-ms-long pulses, and eight 25-ms-long pulses. The time between the pulses was kept large (a few seconds). Figure 3 also shows the probability of crystallization versus the accumulated irradiation time for these pulse schemes. Based on Fig. 2 and Fig. 3, we draw the following conclusions:

1. There is a high resistance to crystallization because of extremely low nucleation probability. On formation of a nucleation center the crystallization process proceeds very rapidly as evidenced by very sharp jumps in the reflected signal in Fig. 2.
2. There is an extremely small probability of crystalline mark formation under ~ 38 ms irradiation time and 100% probability of crystalline mark formation for 200 ms irradiation time. The average nucleation time, the time in which the probability of crystallization reaches 0.5, is ~ 130 ms.
3. The nucleation time seems to be accumulative in nature. When crystallization does not occur during the first (or first few) pulse(s), the irradiated spot seems to have a kind of memory of the irradiation time. That is why all the probability curves fall approximately together in Fig. 3. Previously, we have shown that a controlled laser heating of an amorphous stochiometric PC film ($Ge_2Sb_{2.3}Te_5$) below its crystallization temperature modifies its amorphous state, such that the new amorphous state, called the primed state, has improved the crystallization properties.[5] It may be possible that the amorphous spot having irradiation memory is a material state equivalent to the primed state of stochiometric PC film.

B. Crystalline-Mark Formation on Melt-Quenched Amorphous Film

The study of the crystallization behavior of the melt-quenched amorphous state is important, because in a real system it is the melt-quenched amorphous mark that is going to be erased (or crystallized) in a direct overwrite application. We know that in a stochiometric PC film the crystallization properties of as-deposited and melt-quenched states are significantly different. To investigate if $Ge_5Sb_{68}Te_{27}$ films also show similar difference, we prepared a large melt-quenched amorphous region. This was done by preparing a large crystalline region by scanning the focused laser beam in cw mode at 3.0 mW of power across the PC film in a raster (or a snake) pattern. On this crystalline film surface we wrote an array of very closely spaced melt-quenched amorphous marks by pulsing laser 1 at 16.0 mW. The pulse duration was kept very short (40 ns) for a rapid quenching.

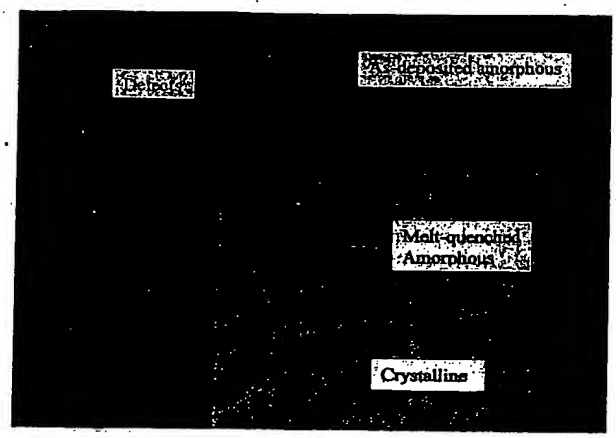

Fig. 4. Picture showing as-deposited amorphous, melt-quenched amorphous, and crystalline sections on a $Ge_5Sb_{68}Te_{27}$ film. The crystalline section was prepared by x–y scanning of a cw laser beam focused on an as-deposited amorphous surface. The melt-quenched amorphous area is created by writing an array (40 × 80) of closely spaced melt-quenched amorphous marks on a crystalline film surface. Focused laser pulses of 16.0 mW and 40-ns long wrote individual melt-quenched marks. The mark spacing in the array is 0.5 μm. We also see some defects on the film, which might have occurred during deposition.

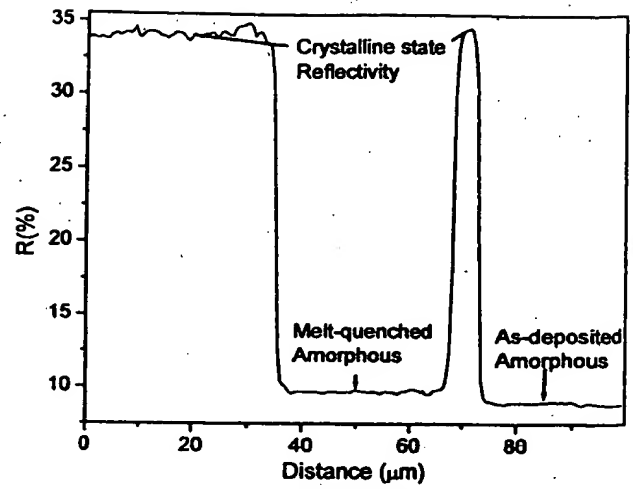

Fig. 5. Reflectivity variation across the film surface shown in Fig. 4. Reflectivity variation was measured by a focused cw laser beam operating at very low power. This graph indicates that the reflectivity of the melt-quenched amorphous state is slightly higher than the as-deposited amorphous state.

The spacing between adjacent marks was smaller than the diameter of individual marks. This ensured a uniform melt-quenched amorphous area. Figure 4 shows a section of the melt-quenched amorphous region created by this method. Such a large melt-quenched amorphous region is impossible to form in a film of stochiometric composition in which any attempt to write an array of melt-quenched marks partly or fully crystallizes previously written marks falling in the vicinity of the focused laser spot. This is because the Gaussian temperature profile around the focused laser spot on the film extends far beyond the size of the molten pool created by the laser heating, which allows nucleation and subsequent growth of crystalline clusters in the periphery of any newly formed melt-quenched mark. However, in $Ge_5Sb_{68}Te_{27}$ material the nucleation probability is extremely small, therefore it is extremely unlikely that any nucleation center is created within 40 ns of the time of the pulse width.

We measured the reflectivity variation of the surface shown in Fig. 4 by scanning a low-power (0.1 mW) focused cw laser 1 beam from approximately the center of the crystalline area toward the top, passing through the melt-quenched area. The result is shown in Fig. 5. This curve indicates that the reflectivity of the melt-quenched amorphous state is slightly higher than the reflectivity of the as-deposited amorphous state. At present we do not unambiguously understand the origin of this difference in reflectivity. However, the nucleation probability of the melt-quenched state is also slightly higher than that of the as-deposited state, which Zhou *et al.*[3] has attributed to the presence of quenched-in embryos in the melt-quenched state. These quenched-in embryos may be responsible for this slight increase in the reflectivity in the case of the melt-quenched amorphous state.

Figure 6 shows the variation in reflectivity during crystalline-mark formation on melt-quenched amorphous film upon application of ten identical laser pulses from laser 1 at ten different spots on the film. All laser pulses have 3.0 mW of power and were 300 ms long (0–300 ms on the x axis). Figure 6 shows an abrupt rise in the reflectivity at the beginning of the laser pulse ($t = 0$) and another jump in reflectivity that occurs randomly anywhere during the pulse. As explained before, the rise in the reflectivity in the

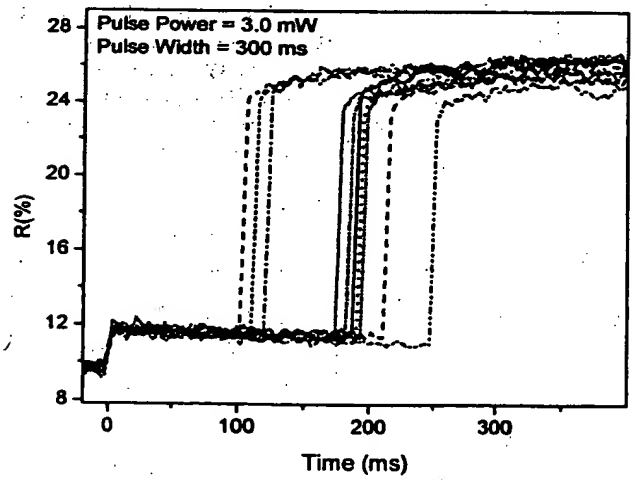

Fig. 6. Reflectivity traces obtained during crystalline mark formation in melt-quenched $Ge_5Sb_{68}Te_{27}$ film in a quadrilayer structure. All crystalline marks were written by a single 3.0-mW laser pulse. The pulse duration was 300 ms (0–300 ms along the x axis). A 0.2-mW cw laser beam from the second laser monitors the reflectivity variation.

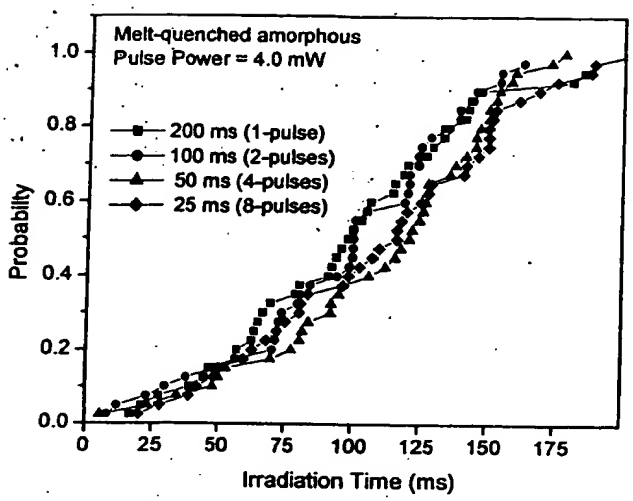

Fig. 7. Probability of crystallization versus irradiation time for various 4.0-mW laser-pulse schemes. In the case of irradiation from multiple pulses, the time interval in between pulses is a few seconds and is not counted in the total irradiation time.

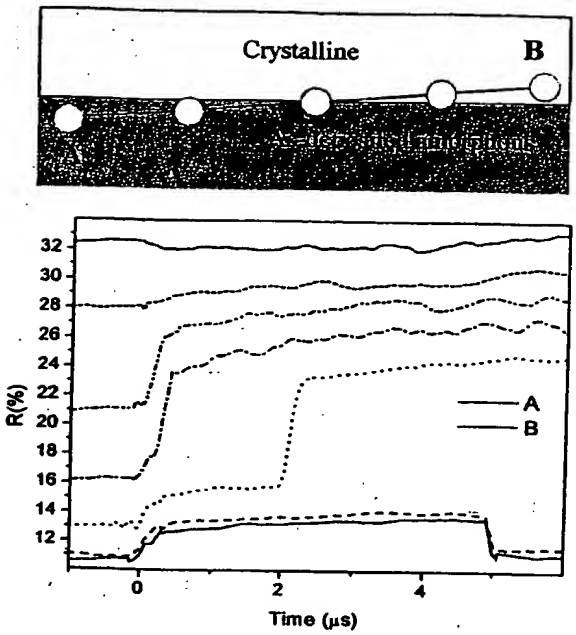

Fig. 8. Schematic of a crystallization experiment conducted at the boundary of the as-deposited amorphous and crystalline $Ge_5Sb_{68}Te_{27}$ film. Open circles indicate laser spots that have a different overlap with the amorphous and crystalline sections as we move along the line AB. The reflectivity curves obtained on application of 4.0-mW, 5.0-μs long laser pulses along this line are also shown. The bottom curve is obtained from spot A, which is in the fully as-deposited amorphous section, and the top curve is obtained from spot B, which is in the fully crystalline section.

beginning of the pulse is not due to the crystalline mark formation, but because of the change in the optical constant of the PC film due to laser heating. Crystallization occurs during the second random jump in reflectivity. Similar experiments carried out at a different pulse power indicate similar behavior. In Fig. 3 we have shown results of a multi-pulse crystallization experiment on as-deposited amorphous film. We conducted an identical experiment on a melt-quenched amorphous surface and the results are shown in Fig. 7. Comparisons of reflectivity traces of Fig. 2 and Fig. 6, and the probability curves of Fig. 3 and Fig. 7 indicate that the fundamental nature of the crystallization kinetics remains approximately same for as-deposited and melt-quenched amorphous states. The only difference between Figs. 3 and 7 is that in case of melt-quenched amorphous film, there is a slightly higher crystallization probability at lower irradiation times, which may be due to the presence of quenched-in embryos in melt-quenched state as indicated by Zhou *et al.*[3]

C. Crystallization at Amorphous and Crystalline Boundary

Figure 8 shows the crystallization experiment conducted at the boundary of as-deposited amorphous and crystalline sections of a PC film ($Ge_5Sb_{68}Te_{27}$) to study the effect of such a boundary on crystalline growth. Many identical 4.0-mW- and 5.0-μs-long pulses from laser-1 were used to write crystalline marks along the line AB in Fig. 8. On moving along the line the overlap of the laser spot increases with the crystalline section. The reflectivity traces obtained during this experiment are also shown in Fig. 8. The bottom two reflectivity traces, where there is no jump in the reflectivity during the laser pulse that indicates no crystalline mark formation. This is because the laser spot was completely in the as-deposited amorphous region, where the probability of crystallization is extremely small for 5.0 μs of irradiation time. Once the laser spot partially moves into the crystalline region, we notice a jump in the reflectivity during the pulse in the third trace from the bottom and also an increase in initial value of reflectivity. The initial reflectivity is the measure of the overlap between the laser spot and the crystalline section because of the fact that the crystalline section has a higher reflectivity as compared to the as-deposited amorphous state. The jump at ~ 2.0 μs indicates crystallization, which is the first crystallization event noticed on moving along the line. On further increasing the overlap of the laser spot with the crystallized portion, we see that the crystallization onset moves toward the onset of the laser pulse. When the laser spot completely moves into the crystalline section (at point B), we see high initial reflectivity, which slightly decreases at the laser pulse onset and thereafter stays constant. This slight drop in the reflectivity at the laser pulse onset is due to a change in the optical constant of the crystalline PC layer due to laser heating. This experiment clearly demonstrates the role of the amorphous-crystalline boundary in the crystallization kinetics of $Ge_5Sb_{68}Te_{27}$ material.

Figure 9 shows the result of an exactly similar experiment carried out at the melt-quenched amorphous and crystalline boundary. Many identical 4.0-mW- and 5.0-μs-long pulses from laser 1 were

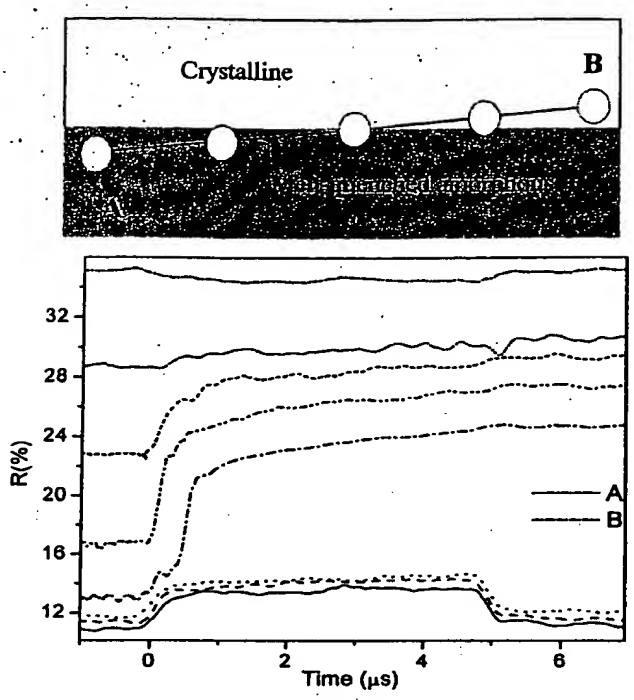

Fig. 9. Schematic of a crystallization experiment conducted at the boundary of the melt-quenched amorphous and crystalline $Ge_5Sb_{68}Te_{27}$ film. Open circles indicate laser spots, which have a different overlap with the amorphous and crystalline sections as we move along the line AB. The reflectivity curves obtained on application of 4.0-mW and 5.0-μs long laser pulses along this line are also shown. The bottom curve is obtained from spot A, which is in the fully melt-quenched amorphous section, and the top curve is obtained from spot B, which is in the fully crystalline section.

used to create crystalline marks along the line AB in Fig. 9. In this figure the bottom three reflectivity traces correspond to no crystalline mark formation because the laser spot was completely in the melt-quenched region. Once the laser spot partially moves into the crystalline region in the fourth reflectivity trace from the bottom, crystallization onset occurs at ~ 0.2 μs. By further increasing the overlap of the laser spot with the crystallized portion, we see that the crystallization onset occurs almost at the onset of the laser pulse. Once the laser focus spot moves into the crystalline section, we see reflectivity traces identical to the one observed in Fig. 8. This experiment clearly indicates that the boundaries of the as-deposited amorphous and the melt-quenched amorphous within the crystalline sections play similar roles in crystallization kinetics.

D. Erasure of Melt-Quenched Amorphous Marks

To study the erasure of melt-quenched amorphous marks, we created three sets of melt-quenched amorphous marks on a fully crystalline $Ge_5Sb_{68}Te_{27}$ film. The first set of melt-quenched amorphous marks were created by operating laser 1 at 16.0 mW pulse power and 40 ns pulse width. These amorphous marks were then erased (re-crystallized) at various pulse power in the range of 2.0–7.0 mW. All erase pulses were 2.0-μs long. The reflectivity traces obtained during this experiment are shown in Fig. 10(a), where the reflectivity trace that shows a drop in reflectivity from ~ 34% to ~ 24%, a difference of 10%, is obtained during melt-quenched amorphous mark formation. The difference between the crystalline-state reflectivity and the reflectivity measured at the center of the melt-quenched mark on the crystalline surface by a focused laser spot having a Gaussian intensity profile is the measure of the size of the melt-quenched amorphous mark. Larger amorphous marks will have a larger overlap with the laser spot, therefore will show a larger drop in the reflected intensity. The reflectivity traces obtained during the erasure of these marks at various pulse power indicate that a minimum pulse power of ~ 4.3 mW is needed to erase these marks. This is because lower values of pulse power do not produce enough temperature at the mark boundary to trigger crystalline growth. As indicated earlier, the laser spot has a Gaussian intensity distribution at the focus, which produces a radially symmetric Gaussian temperature distribution at the mark center and the height of the Gaussian temperature profile is proportional to the pulse power. The temperature profiles can be simulated using a computer code TEMPROFILE™.[10] Commercial quadrilayer structures, such as the one used in this study are designed to reach a steady-state temperature distribution under 1.0 μs of laser irradiation. Based on this analysis, we conclude that 4.3 mW of pulse power raises the temperature at the mark boundary to a value at which there is a slight growth probability to initiate the erasure of the melt-quenched mark. The erasure of the melt-quenched amorphous mark occurs by inwards growth of the crystalline boundary. Above 4.3 mW of pulse power, we see that crystallization onset time decreases with increasing the pulse power. For a very high erase pulse power (7.0 mW) setting we see that the crystallization starts at the onset of the laser pulse. At this power, the temperature at the mark boundary quickly reaches a value at which there is a very high crystalline growth probability.

The second set of marks was created by laser pulses having 14.5 mW of pulse power and 40-ns pulse width. Reflectivity traces obtained during the melt-quenched amorphous mark formation and erasure of these amorphous marks by 2.0-μs-long pulses having variable power are shown in Fig. 10(b). These amorphous-mark sizes are smaller as indicated by a 9% drop in the reflectivity, which is smaller in comparison with a 10% drop in the reflectivity during the formation of the first set of marks. The minimum pulse power required to erase these marks is 3.9 mW. This is because the mark boundary is closer to the center of the laser focus spot, where a higher temperature can be reached by a relatively lower power laser pulse. Figure 10(c) shows the results of a similar experiment conducted on a third set of melt-quenched amorphous marks created by 12.0-mW, 40-ns laser pulses. The minimum laser power required to erase

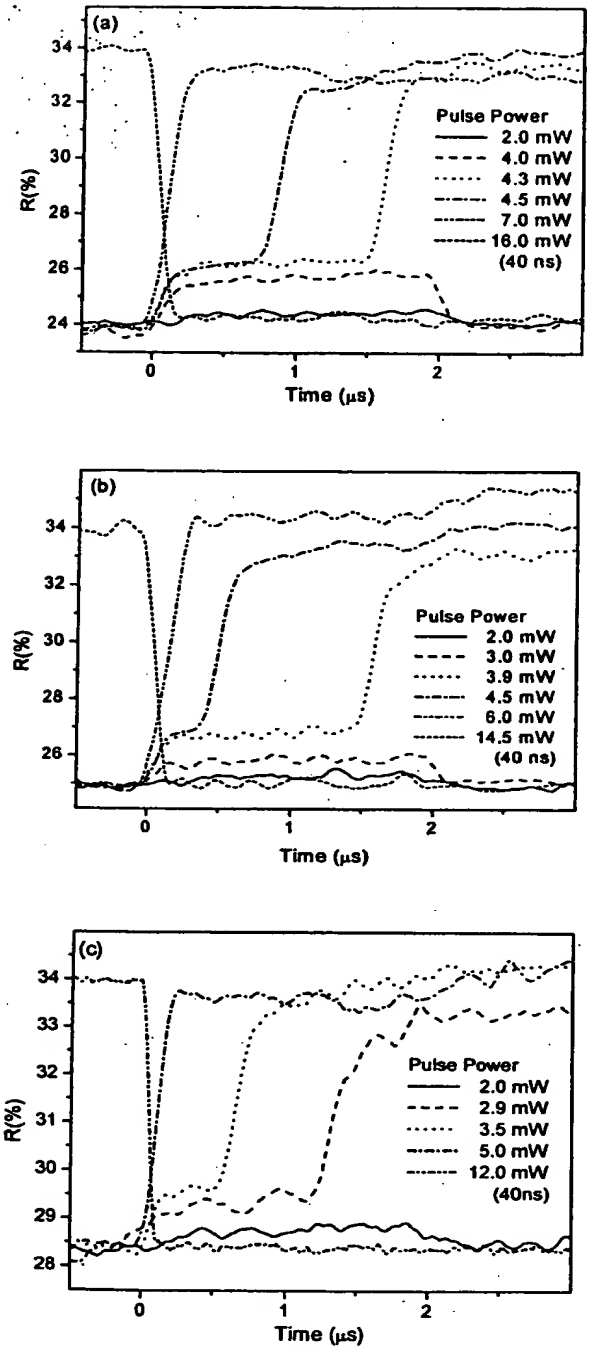

Fig. 10. (a) Reflectivity curves obtained during melt-quenched amorphous mark formation on a fully crystalline $Ge_5Sb_{68}Te_{27}$ film by a 16-mW, 40-ns long laser pulse and during the attempted erasure of this mark at various laser pulse powers. All laser pulses used in the erasure have a 2.0-μs pulse width. (b) Reflectivity curves obtained during melt-quenched amorphous mark formation on fully crystalline $Ge_5Sb_{68}Te_{27}$ film by a 14.5-mW, 40-ns long laser pulse and during the attempted erasure of this mark at various laser pulse powers. All laser pulses used in the erasure have a 2.0-μs pulse width. (c) Reflectivity curves obtained during melt-quenched amorphous mark formation on a fully crystalline $Ge_5Sb_{68}Te_{27}$ film by a 12-mW, 40-ns long laser pulse and during the attempted erasure of this mark at various laser pulse powers. All laser pulses used in the erasure have a 2.0-μs pulse width.

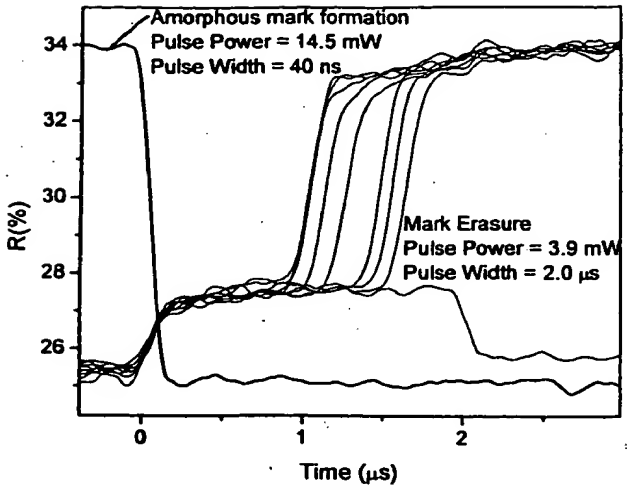

Fig. 11. Reflectivity trace obtained during a melt-quenched amorphous mark formation by a 14.5-mW, 40-ms laser pulse shows a drop in reflectivity from 34% to 25%. If we erase many such melt-quenched marks by 4.3-mW, 2.0-μs long pulses, we obtain the reflectivity variation curves as shown.

these marks is 2.9 mW. Based on the results shown in Figs. 8, 9, and 10, we conclude that in $Ge_5Sb_{68}Te_{27}$ media the mark erasure starts at the crystalline-amorphous boundary once the temperature at the mark boundary is above a certain temperature.

E. Fluctuations in Erasure Onset Time of the Melt-Quenched Marks

In the previous experiment we have shown that the erasure of a melt-quenched amorphous mark starts from the mark boundary once the temperature at mark boundary reaches a critical value. However, the erasure at the critical temperature is probabilistic in nature, which is depicted in Fig. 11. Ten melt-quenched amorphous marks were created by 14.5-mW, 40-ns-long laser pulses on crystalline $Ge_5Sb_{68}Te_{27}$ film. All of these marks were then erased by 3.9-mW, 2.0-μs-long laser pulses. The reflectivity traces obtained during melt-quenched amorphous-mark formation and during erasures are shown in Fig. 11. This figure shows that the erasure onset time for nine melt-quenched amorphous marks fluctuates between 0.9 to 1.6 μs (in one of the cases there was no erasure). We know that formation of nucleation centers and their subsequent growth are probabilistic processes, which are functions of temperature.[11] At lower temperature there is a small growth probability, therefore we see a fluctuation in crystallization onset time. On increasing the pulse power, the temperature at the mark boundary increases to higher value, and we see a consistent erasure of the melt-quenched marks at the onset of the laser pulse.

F. Amorphous-Mark Erasure in Nucleation-Dominated and Growth-Dominated Phase Change Films

Figure 12(a) shows variation in the reflected signal during the erasure of various sizes of melt-quenched

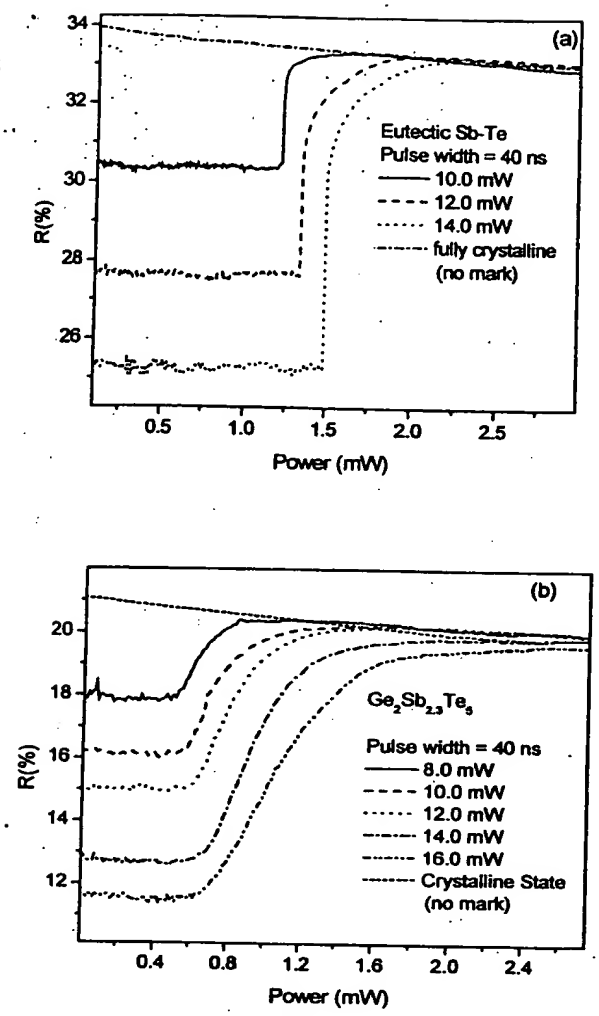

Fig. 12. Variation in the reflected signal during the erasure of various size melt-quenched amorphous marks in (a) eutectic $Ge_5Sb_{68}Te_{27}$ alloy film and (b) stochiometric Ge-Sb-Te alloy film. Various size amorphous marks were created on crystalline films by 40-ns long laser pulses at various pulse powers as indicated. These melt-quenched amorphous marks were erased by slowly increasing the cw power of laser 1, while laser 2 operating at a fixed low cw power (0.1 mW) was used for measuring the reflected signal.

amorphous marks written on a crystalline $Ge_5Sb_{68}Te_{27}$ film sample by a focused cw laser beam. These amorphous marks were created by 40-ns-long laser pulses of 10, 12, and 14 mW of pulse power. As mentioned earlier, a higher pulse power forms a bigger melt-quenched amorphous mark and gives rise to a lower reflectivity at the mark center. In all cases after the formation of a melt-quenched amorphous mark, it was erased by slowly increasing the cw power of same laser in steps of 0.01 mW, while a second focused cw laser beam operating at a constant, very low power monitored the variation in the reflected signal. In Figure 12(a) we observe that on increasing the cw power, the reflected signal suddenly increases at some critical power, and the value of this critical power increases with the mark size. In this experiment the rate of increase of the erase power is very small, therefore for a given value of a cw power there is a radial distribution of steady-state temperature around the center of the amorphous mark. For bigger marks the critical temperature at the mark boundary is achieved at a higher laser power. Thus the reflectivity variation results shown in Fig. 12(a) further confirm our previous results that crystallization proceeds from the amorphous-crystalline boundary once the temperature at the boundary reaches a critical value.

A similar experiment has been conducted on a $Ge_2Sb_{2.3}Te_5$ film whose composition is close to the stochiometric ratio. The results of this experiment are shown in Fig. 12(b), which shows that the erasure of the amorphous mark occurs at a relatively lower power and at approximately the same power for all sizes of amorphous marks. This indicates that the mark boundary has no role to play in the process of crystallization of this film. In this case crystallization starts at the center of the amorphous mark by the formation of several nucleation centers. Subsequently, these nuclei grow independently to form crystalline clusters until the entire amorphous mark is crystallized. Because the nucleation occurs at a lower temperature, we see crystallization onset at a lower laser power. Further, in this film crystallization speed is significantly smaller as indicated by a slower rate of increase in the reflectivity after the crystallization onset. A linear drop in R in all the reflectivity traces on completion of the erasure of amorphous marks in Figs. 12(a) and 12(b) is due to a continuous change in the optical constants of the crystallized PC film as the increasing laser power continues to raise the temperature at the focus spot. The topmost curves in both figures represent the erasure of an amorphous mark of zero size (or the heating of a fully crystalline film).

G. Composition Dependence of the Crystallization Behavior

Several PC materials can be made for optical data storage application by varying the Sb/Te ratio and the amount of Ge doping in the vicinity of the eutectic point $Sb_{70}Te_{30}$. All of these materials show growth-dominated crystallization kinetics. The importance of high nucleation time has been stated in the introduction in Section 1, which leads to very high mark of stability, low jitter, and the capability to write a smaller mark for a higher recording density. However, crystallization speed is another important parameter for optical data storage application. Higher crystallization speed would lead to a faster erasure of a melt-quenched amorphous mark, which would give a higher overwrite speed for rewritable disk application. Therefore, an ideal PC material for optical data storage would be the one that has a large incubation time and a very high crystallization speed. We have studied several binary and ternary alloys to investigate the effect of the variation of the Sb/Te ratio and of Ge doping on incubation time and crys-

Table 1. Description of Samples Used[a]

Binary Sample	Sb/Te Ratio	Ternary Sample	Sb/Te Ratio
$(Sb_{86.7}Te_{13.3})$	~6.52	$(Ge_{3.5}Sb_{85.5}Te_{11.0})$	~7.77
$(Sb_{81.5}Te_{18.5})$	~4.41	$(Ge_{4.3}Sb_{81.5}Te_{14.2})$	~5.74
$(Sb_{73.8}Te_{26.2})$	~2.82	$(Ge_{4.8}Sb_{79.0}Te_{16.2})$	~4.88
		$(Ge_5Sb_{68}Te_{27})$	~2.52

[a]To study the effect of the Sb/Te ratio and Ge doping on crystallization kinetics.

tallization speed. Table 1 gives the description of samples used in this investigation. Figure 13(a) shows the probability of crystalline-mark formation on as-deposited amorphous film of one of the samples $(Sb_{86.7}Te_{13.3})$ listed in Table 1 at various pulse powers, which indicates that the average incubation time to start crystallization falls in the 1.8–2.7 μs range. Here the average incubation time is the time in which the crystallization probability reaches 0.5. Figure 13(b) shows the reflectivity traces at various pulse powers. Because there is a large fluctuation in the crystallization onset time, we have used only those curves that show crystallization onset in the vicinity of 1.2 μs at a particular pulse power. Therefore, any individual curve in Fig. 13(b) is obtained after many crystallization attempts. This is done to ensure that, at the time of crystallization onset, the temperature remains proportional to the applied pulse power. The vertical scale in Fig. 13(b) is normalized in the range of 0–1, where 0 represent the amorphous state reflectivity and 1 represents the reflectivity of fully crystalline film. This normalization is required to compare the crystallization speed of various samples of different compositions listed in Table 1, which have different reflectivities in their crystalline

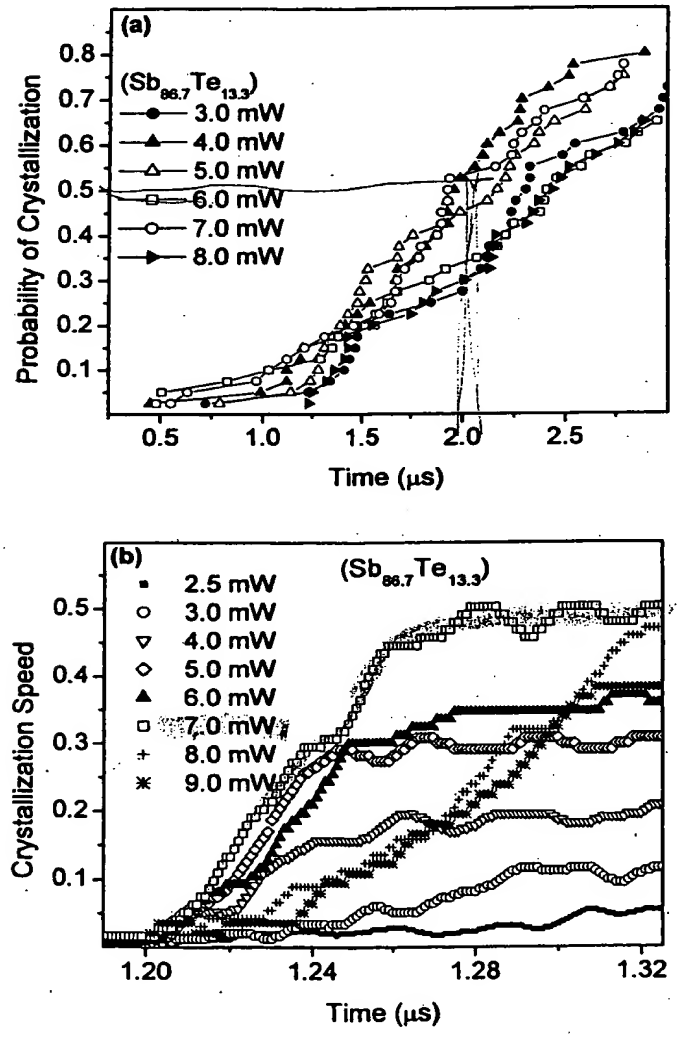

Fig. 13. (a) Probability of crystalline mark formation versus the duration of the pulses at various laser pulse power in sample $Sb_{86.7}Te_{13.3}$. (b) Crystallization growth rate (or speed of crystalline mark formation) at various laser pulse power in sample $Sb_{86.7}Te_{13.3}$. Amorphous and crystalline state reflectivities are scaled in the range 0 to 1.

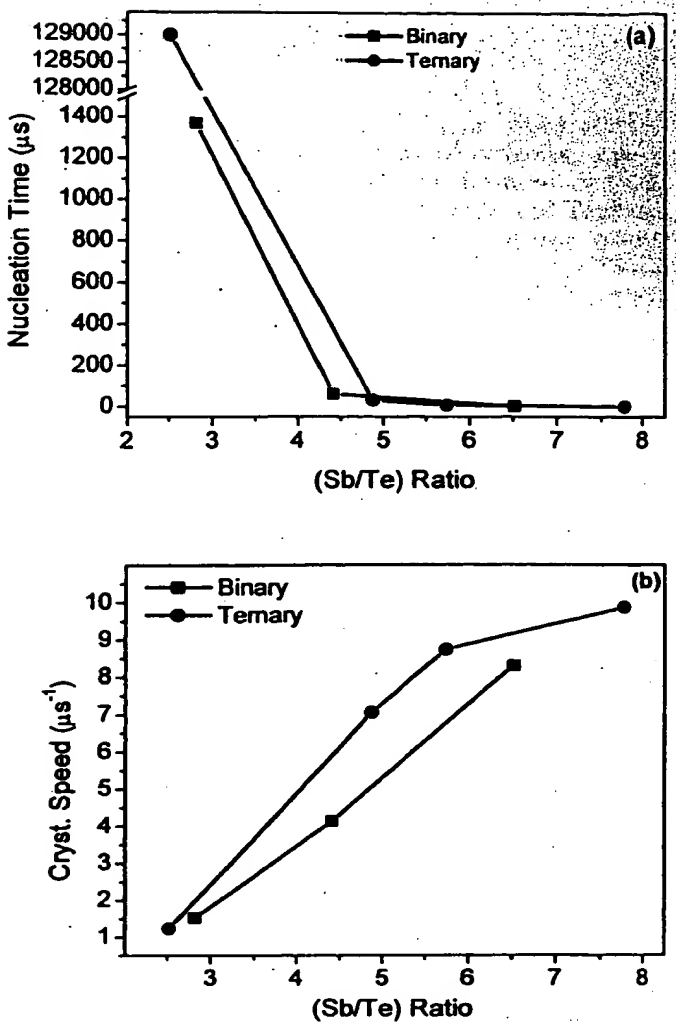

Fig. 14. Comparison of the variation in (a) nucleation time and (b) crystalline growth rate as a function of the Sb/Te ratio in binary and ternary alloys.

and amorphous states. The crystallization speed is measured in the time range where the reflected signal lies in between 40–60% of its maximum value in any individual trace. In case of Fig. 13(b), the maximum crystallization speed was obtained at 7.0 mW. Similar experiments were conducted on two other binary alloys and four ternary alloys listed in Table 1, which also indicates the composition ratio for each sample. Figure 14(a) and 14(b) is the graphical representation of the variation in nucleation time and crystallization rate as a function of the Sb/Te ratio. Figure 14(a) shows that for the Sb/Te ratio higher than ~ 4.5, the nucleation time for both binary and ternary alloys is approximately the same. On decreasing the Sb/Te ratio below 4.5, we observe a very sharp rise in nucleation time. Figure 14(b) shows that on increasing the Sb/Te ratio, the crystallization speed increases in both binary and ternary alloys, and that the crystallization growth rate is slightly higher for the ternary alloy system at a given Sb/Te ratio. In comparison with these eutectic binary and ternary materials, the nucleation time for the stochiometric GeSbTe material is less than 10 ns, and it has a maximum growth rate ~ $2.79/\mu s^{-1}$.

4. Conclusions

We have presented a set of experiments that show that in eutectic Sb–Te based alloys the initiation of the crystallization process in fully as-deposited and melt-quenched amorphous states is extremely slow because of a large nucleation time. Though there is a slight improvement in the nucleation probability in the melt-quenched state, the basic crystallization kinetics remain very similar in both states. Both states show excellent crystalline growth at the amorphous-crystalline boundary (a situation of relevance in a real data storage system), which makes these alloys very useful for direct overwrite optical data storage devices. We have also shown that the nucleation probability is a function of the accumulative laser irradiation time, which means that it does not matter if we irradiate the film continuously in one step or in small steps with large ideal time intervals. This study also indicates that on increasing the incubation time by decreasing Sb/Te ratio, crystallization speed decreases. Therefore, one has to set a compromise between incubation time and crystallization speed. It seems that the Sb/Te ratio somewhere in between 4.5 to 5 would be an optimized value for the Sb/Te ratio. Once the Sb/Te ratio is optimized, a doping of an appropriate amount of Ge may be done to increase the crystallization speed. It would be worthwhile to do jitter measurements in the vicinity of the Sb/Te ratio at ~ 4.5 to determine the exact composition of the alloy to optimize the disk performance.

This work has been sponsored by the Optical Data Storage Center at the University of Arizona, and in part by a grant from the U.S. Department of Commerce's National Institute of Standards and Technology under Advanced Technology Program award number 70NANB7H3054. We also thank T. Ohta in Matsushita Electric Industrial Co., Ltd. for providing some of the samples used in this study.

References

1. N. Yamada, E. Ohno, K. Nishiuchi, and N. Akahira, "Rapid-phase transition of GeTe–Sb_2Te_3 pseudobinary amorphous films for optical disk memory," J. Appl. Phys. **69**, 2849–2856 (1991).
2. H. Iwasaki, M. Harigaya, O. Nonoyama, Y. Kageyama, M. Takahashi, K. Yamada, H. Deguchi, and Y. Ide, "Completely erasable phase change optical disk II: Application of Ag-In-Sb-Te mixed-phase system for rewritable compact disc compatible with CD-velocity and double CD-velocity," Jpn. J. Appl. Phys. **32**, 5241–5247 (1993).
3. G. F. Zhou, H. J. Borg, J. C. N. Rijper, M. H. R. Lankhorst, and J. J. L. Horikx, "Crystallization behavior of phase change materials: comparison between nucleation- and growth-dominated crystallization," in *Optical Data Storage 2000*, D. G. Stinson and R. Katayma, Proc. SPIE **4090**, 108–117 (2000).
4. M. Horie, T. Ohano, N. Nobukuni, K. Kiyano, T. Hashizume, and M. Mizuno, "Material characterization and application of eutectic SbTe based phase-change optical recording media," in *Optical Data Storage 2001*, T. Hurst and S. Kobayashi, eds., Proc. SPIE **4342**, 76–87 (2002).
5. P. K. Khulbe, E. M. Wright, and M. Mansuripur, "Crystallization behavior of as-deposited, melt-quenched, and primed amorphous states of $Ge_2Sb_{2.8}Te_5$ films," J. Appl. Phys. **88**, 3926–3933 (2000).
6. E. M. Wright, P. K. Khulbe, and M. Mansuripur, "Dynamic theory of crystallization in $Ge_2Sb_{2.8}Te_5$ phase-change optical recording media," Appl. Opt. **39**, 6695–6701 (2000).
7. M. Mansuripur, J. K. Erwin, W. Bletscher, P. Khulbe, K. Sadeghi, X. Xun, A. Gupta, and S. Mendis, "Static tester for characterization of phase-change, dye-polymer, and magneto-optic media of optical data storage," Appl. Opt. **38**, 7095–7104 (1999).
8. N. Akahira, N. Miyagawa, K. Nishiuchi, Y. Sakaue, and E. Ohno, "High-density recording on phase-change optical disks," in *Optical Data Storage '95*, G. R. Knight, H. Ooci, and X.-S. Tyan, Proc. SPIE **2514**, 294–302 (1995).
9. P. K. Khulbe and M. Mansuripur, "Temperature-dependence of optical constants in phase-change media," Technical Digest, Optical Data Storage Topical Meeting 2001, 121–123 (2001).
10. TEMPROFILE™, a product of MM Research, Inc., Tucson, Ariz.
11. J. W. Christian, *The Theory of Transformations in Metals and Alloys*, 2nd ed. (Pergamon, Oxford, 1975).